18

Miniaturized Version of the STIFF-FLOP Manipulator for Cadaver Tests

Giada Gerboni, Margherita Brancadoro, Alessandro Diodato, Matteo Cianchetti and Arianna Menciassi

The BioRobotics Institute, Scuola Superiore Sant'Anna,
Pontedera (PI), Italy

Abstract

The previous version of the STIFF-FLOP manipulator (reported in Chapters 2 and 3) has demonstrated to have all the capabilities to perform an effective surgical operation, being able to bend in any direction, to sense the external forces, and to elongate and to change its stiffness. On the other hand, its size is not yet compatible with standard tools used for minimally invasive surgery (i.e., standard trocar ports). The work described in this chapter has focused on the development of a miniaturized version of the STIFF-FLOP manipulator, with limited sensing and stiffening abilities. This manipulator has been equipped with a camera and used in a realistic scenario, such as cadaver tests. The STIFF-FLOP robotic optic arm seemed to acquire superior angles of vision of the surgical field and neither intraoperative complications nor technical failures were recorded.

18.1 Requirements for Manipulator Usability in Cadaver Tests

The miniaturized version of the soft manipulator has been designed taking advantage of the expertise gained in developing previous STIFF-FLOP manipulator versions. Modularity, novel actuation technologies, and smart geometries have been exploited to match the following specific requirements:

- The entire device has to fit the maximum size of traditional trocars, and thus a diameter smaller than 15 mm is strictly required.

- The manipulator should allow adjusting the position and direction of the end-effector separately, by keeping the shaft stable; thus more than four degrees of freedom (DOFs) are necessary to enable the required flexibility. This means that at least two modules, each one integrating a 4-DOF flexible fluidic actuator (FFA), are required.
- The employed FFA must not generate free elastomeric deformation phenomena (e.g., lateral chamber expansions, ballooning, etc.) during its use. This would ensure a reduced risk of breakage and an efficient use of fluidic actuation.
- The compliance of the soft modules must be preserved as much as possible in order to squeeze out the deflated manipulator from tight spaces in case of emergency.
- A free lumen of about 4–5 mm is required for feeding through surgical tools (e.g., laparoscopic graspers, RF tools, etc.), or for allocating the wires of a laparoscopic camera for vision, which can be fixed at the tip.
- The manipulator maneuverability must take into account the effect of downline loads, including the weight of additional modules.
- The manipulator has to be able to exert forces and handle unwanted contacts while maintaining the distal extremity (where the guided surgical tool is located) at the required position for accomplishing the surgical task.

For the STIFF-FLOP arm version used for cadaver tests, the efforts have been mainly focused on replicating the mobility performances already obtained with the previous large versions of the STIFF-FLOP arms, but at a smaller scale.

18.2 System Adaptation

Figure 18.1 shows the design of the whole miniaturized STIFF-FLOP manipulator system, which is composed of two pneumatically actuated hollow modules. The manipulator is attached to a rigid shaft, which is also hollow and serves as support during the MIS procedure. This rigid shaft connects the flexible manipulator to the pressure-control system and it is necessary to rigidly interact with the fulcrum at the entry port where the trocar is placed. The shaft can be controlled either manually by the medical personnel or by a robot.

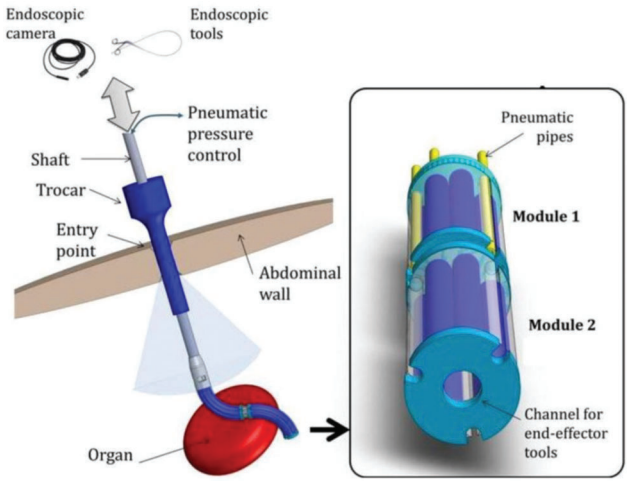

Figure 18.1 (Left) Envisaged system applied to a MIS scenario. (Right) Manipulator design with two soft modules able to bend in every direction and elongate (4 DOF).

The two modules, as specified in Figure 18.1 – right, are both able to perform omnidirectional bending and elongation motion in response to the level of pressure applied to their inner chambers. A thin and hollow connection merges the two modules while keeping the chambers of the two modules aligned.

The first module is rigidly connected to the shaft in which the six fluidic pipes are guided to reach the external pressure control system. The pipes from the second module are guided along the outer walls of the first module not to occupy the inner lumen, which must be preserved for feeding surgical instruments or camera wires. Then all the pipes of all the modules are guided through the hollow shaft connecting the chambers to the external pressure control system.

Figure 18.2 shows a detailed view of a single module, which is 50 mm in length and 14.5 mm in external diameter, making it suitable for MIS applications employing standard trocars. The module contains three pairs of pneumatic chambers measuring 3 mm in diameter, designed with the approach detailed in Chapter 3.

As visible in Figures 18.1 and 18.2, a module is made up of six cylinders. This is because for each DOF, a pair of chambers is engaged. This choice is due to the fact that the module has to preserve a reasonably large hollow lumen (4.5 mm in diameter) for feeding through instruments (or devices or

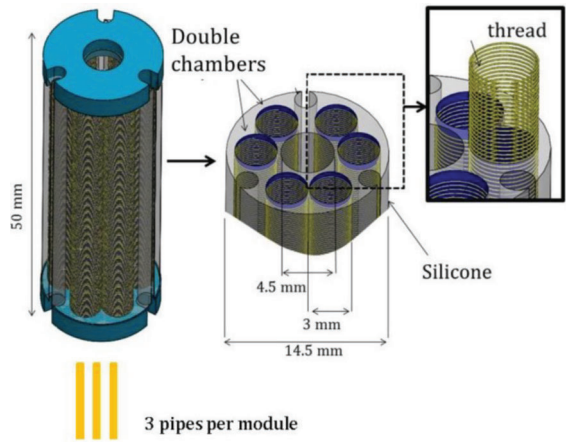

Figure 18.2 Single-module design with relevant quotes. The section view in the middle shows the inner arrangement of the chambers. The inset shows an exploded view of the thread used for avoiding the lateral chamber expansion.

stiffening mechanisms), and thus the residual space left in the module limits the maximum diameter of the chamber's circular cross section. Hence, in order to fill up the space available with cylindrical chambers, two cylinders of a smaller diameter are used in parallel for each DOF. An internal pipe connects the two chambers related to the same bending motion; so the pair of chambers can be considered as a single larger chamber, which is inflated by just one pipe from the central pressure-control system. Two end caps, made of a stiffer silicone (depicted in blue in Figure 18.2), are included at the top and bottom parts of the module, hermetically closing the chambers. The bottom of the module is designed to embed also the three pipes for the pneumatic pressure supply of each pair of cylindrical chambers.

In order to maintain the inner central lumen free, the module design includes three little external grooves in the silicone body for allocating the pipes coming from the distal module. In these grooves, the pipes can easily slide longitudinally while the module is working (bending and elongating). The grooves are shaped such that the pipes cannot escape from them. In case of more than two modules, a more efficient management of pipes coming from the distal modules should be identified.

The detailed manufacturing process of the small-sized modules of the STIFF-FLOP arm for cadaver tests follows the same strategy of the large-scale modules previously described in Chapter 3.

18.3 System Modeling and Characterization Methods

The miniaturized version of the manipulator intended for cadaver tests does not include an active system for stiffening (i.e., the granular jamming chambers). The elongation/bending actuation by itself produces some structure stiffening, which can be quantified. For this reason, the manipulator was modeled in order to characterize the stiffness of the single module when actuated [1].

Thanks to this module analysis, it is possible to predict the behavior of the entire manipulator when more modules are combined together: this can be important information for improving the design. Indeed, with such a model, the maneuverability limitations due to downline loads (i.e., the forces applied to the top of the distal module) can be estimated. Therefore, every module can be modeled in relation to the number of modules that follow it. In addition, the fluidic actuation efficiency of the soft module with only cylindrical elongating chambers' design can be evaluated.

Concerning the elongation motion primitive (eMP), the module can be seen as a spring, having constant K_L, which can elongate thanks to the force generated by the same pressure applied into all the six (2×3) chambers. Hence, the balance of the forces acting on the module during the eMP can be expressed as in Equation (18.1) (Figure 18.3 – left). The external loads are expressed by F_e.

The bending motion primitive (bMP) envisages a balance of the torque values around the base of the module. In this case, the module appears as a torsional spring, having constant K_t, which rotates by an angle θ when a single pair of chambers is inflated with pressure P. Considering the complexity of precisely modeling the module's actuation, a linear dependency of the resulting torque from the imposed chamber pressure was assumed. The balance of torque values, including the external torque (τ_e), is expressed as in Equation (18.2) (Figure 18.3).

Factor γ in Equation (18.1) represents the efficiency of the actuation. In every actuator, not all the input energy is totally converted into the output energy as part of this energy is dissipated through various phenomena (including friction, defects, leakages, and heat). Parameter α in Equation (18.2) is an unknown parameter, which takes into account the actuation efficiency and the chambers' contact area and arm with respect to the central axis.

In order to estimate the parameters of the model in Equations (18.1) and (18.2) (i.e., elastic constants K_L and K_t and factors γ and α), dedicated experimental tests have been carried out.

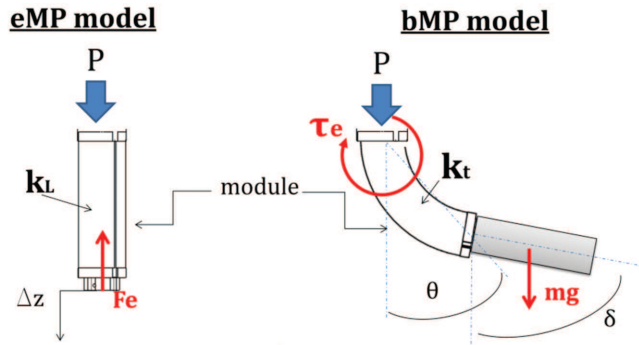

$$PA\,\gamma = k_L \Delta z + F_e \quad \text{Equation (18.1)}$$

$$A = 6A_c \quad \text{Equation (18.3)}$$

$$P\,\alpha = k_t \theta + \tau_e \quad \text{Equation (18.2)}$$

$$\tau_e = mg\,(L\,\sin\theta + {}^{L}/_{2}\sin\delta) \quad \text{Equation (18.4)}$$

Figure 18.3 (Left) Model of the module during eMP in response to the pressure P supplied to all the chambers. (Right) Model of the module during bMP in response to the pressure P supplied to a single couple of chambers in the proximal module. A_c is the effective area of a single chamber, m and L are, respectively, the mass and the length of a module, θ is the bending angle, and δ is the angle described by the extremities of "external load." The external load is represented by another module having the same dimensions and weight of the first and generates the torque τ_e.

For measuring the displacement of the modules, we used the tracking system Aurora (by NDI medical), provided with small probes (Aurora Mini 6 DOF Sensor 1.8 mm $\times$ 9 mm) positioned on key points of the manipulator.

For the estimation of the parameters of Equation (18.1), two data sets were collected, considering two different eMP conditions:

- **eMP_c1** The module can freely elongate in response to pressure P being supplied to all the chambers (Figure 18.4 – left).
- **eMP_c2** Isometric condition: The module is constrained to its initial length by positioning a ground-fixed load cell (ATI-Industrial Automation F/T sensor nano17) at its top (Figure 18.4 – right).

By applying Equation (18.1) to each of these conditions, the following system holds:

$$\begin{bmatrix} 0 \\ F_e \end{bmatrix} = \begin{bmatrix} PA & -\Delta z \\ PA & 0 \end{bmatrix} \begin{bmatrix} \gamma \\ k_L \end{bmatrix} \tag{18.5}$$

For the estimation of the parameters of Equation (18.2), the following two bending MPs (bMP) were considered:

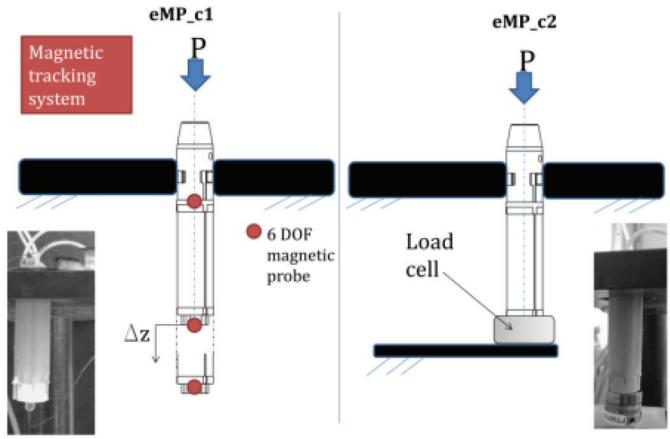

Figure 18.4 (Right) Bench test of the test evaluation of the displacement performed during free elongation motion (eMP_c1). (Left) Bench test of the test for measuring the force exerted by the module in the longitudinal direction on the load cell (eMP_c2).

- **bMP_c1** The module can freely bend in response to pressure P being supplied to a single pair of chambers (Figure 18.5 – left).
- **bMP_c2** The module can bend in response to pressure P being supplied to a single pair of chambers (Figure 18.5 – right). In this case, an external torque is applied. In a realistic scenario, this external torque would be generated by the presence of another module attached, for example, at the top of the first module (Figure 18.5 – right).

By applying Equation (18.2) to each of the above conditions, the following equation can be found:

$$\begin{bmatrix} 0 \\ \tau_e \end{bmatrix} = \begin{bmatrix} P & -\theta_1 \\ P & -\theta_2 \end{bmatrix} \begin{bmatrix} \alpha \\ k_t \end{bmatrix} \tag{18.6}$$

Equations (18.5) and (18.6) have the form:

$$Y = Ax \tag{18.7}$$

These two equations can be solved by using the pseudo-inverse $A\dagger$ approach (least squares method) for estimating the vector parameters.

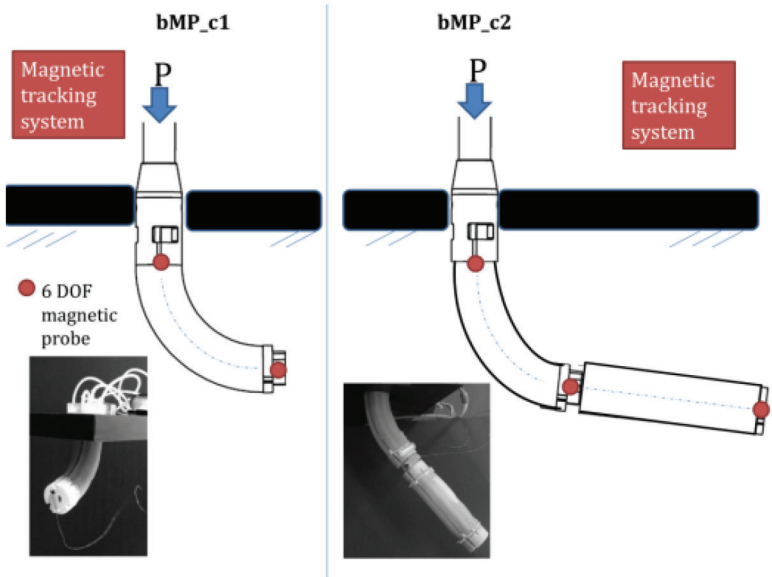

Figure 18.5 (Right) Bench test for the evaluation of the bending angle θ_1 performed during free bending motion (bMP_c1). (Left) Bench test for the evaluation of the bending angle θ_2 performed during loaded bending motion (bMP_c2). In this case, another module, provided with another six DOFs magnetic probe at the top, is used as load.

18.4 Results of Characterization

The results about the tests and model parameters estimation for eMP are summarized in Table 18.1. The module is able to elongate up to 27% during free body elongation, while the maximum force developed along the main axis was recorded to be 3.6 N before buckling phenomenon appears. Table 18.1 also reports the estimation reliability of the eMP model, expressed by Equation (18.1), in predicting the force developed by the module in terms of R^2 and mean and standard deviation of residual errors.

Table 18.1 Test results and model parameter estimation for eMP

Maximum elongation	13.67 mm
Maximum force exerted	3.6 N
γ	0.91
k_L	320.59 N/m
Mean $\pm$ std of residual errors	-0.09 ± 0.2 N
R^2	0.96

The same type of summary regarding the tests and model parameters estimation during bMP is reported in Table 18.2. The maximum angle achieved in unloaded condition (Figure 18.5, left) is 38.46°, while when the load is attached, it reaches 25.9° (Figure 18.5, right), and thus the angular difference between the two conditions is 12.56°. This difference is also reported for the entire data set in Figure 18.6. The estimation reliability of the bMP model is also reported in Table 18.2.

The models developed for the module in both eMP and bMP demonstrated to correctly predict the behavior of the real module. In a sense, this type of analysis allows to estimate the effective workspace of the manipulator, because it considers the effects of all the downline loads possibly applied to each module. In fact, Equations (18.1) and (18.2) could be recursively used for evaluating the force and the torque applied to the tip of each module. The modules are rigidly fixed one to another, and thus it is possible to assume

Table 18.2 Test results and model parameter estimation for bMP

Max free bending angle	38.46°
Max loaded bending angle	25.9°
α	8.15E^{-8} Nm/Pa
k_T	2.27E^{-4} Nm
Mean $\pm$ std of residual errors	$-1.39\text{E}^{-4} \pm 3.84\text{E}^{-4}$ Nm
R^2	0.85

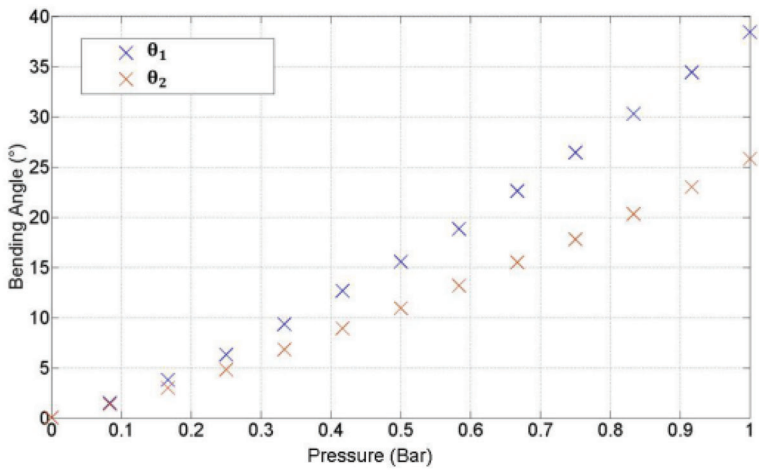

Figure 18.6 Bending angle recorded under the two conditions shown in Figure 18.5: unloaded (blue) and loaded state (orange).

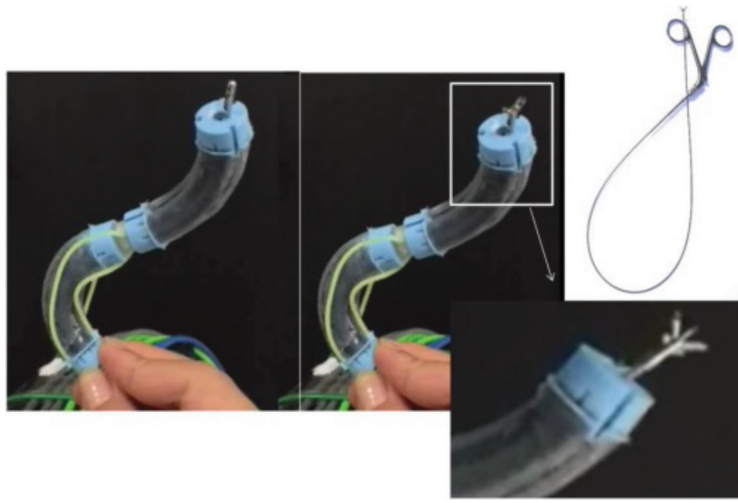

Figure 18.7 The soft manipulator is articulated while carrying a flexible endoscopic instrument (biopsy tool).

equilibrium of force and torque from the one module distal part to the base of the following module. However, two modules are already enough to equip the surgeon with the required flexibility to approach the target.

From Figure 18.6, it is possible to observe the effect of the load on the progression of the bending angle. Indeed, all the values of the free bending angle are bigger than the loaded angles. Furthermore, a relatively high force can be exerted by the module in the axial direction (Table 18.1).

The results about the actuation efficiency γ, reported in Table 18.1, confirm that the use of cylindrical chambers with thread, which do not expand but only elongate, improves the performance of the overall STIFF-FLOP robot system.

Finally, Figure 18.7 shows the manipulator provided with a commercially available flexible biopsy tool for standard endoscopes, demonstrating that the manipulator is able to articulate and withstand loads produced by the flexible instrument inside. The soft manipulator can be therefore used to approach difficult-to-reach targets during MIS procedures in a safe manner.

18.5 Prototype for Cadaver Test (with Integrated Camera)

The previously described two-module manipulator has been equipped with an endoscopic camera and used for tests in human bodies (cadaver tests).

Figure 18.8 shows this manipulator assembled for the cadaver tests and lists the specifications regarding the selected endoscopic camera (by Misumi Electronic Corp.).

In this case, even smaller fluidic pipes (size 1 mm of external diameter) were employed and passed into the lumen of the device. This was to facilitate the passage of the manipulator through the trocar port several times during the operation. In this way, the pipes are more protected and the modules showed an increased robustness.

The aluminum shaft, used for supporting the manipulator, has a diameter of 10 mm, thus allowing easy sliding of the shaft into the 15 mm trocar during the operation.

The entire device is firmly fixed to the operating table attached to an articulated arm (the Martin's Arm or Aurora arm) by means of a 3D printed connection, which also embeds the connection of the pneumatic pipes connecting air chambers with the remote control system and the camera USB connection. Figure 18.9 shows a panoramic view of the operating room, depicting the assembled device attached to the Martin's arm above the table.

Finally, the camera horizon is adjusted with respect to the upward movements of both the modules, once the manipulator is positioned in the appropriate operating configuration.

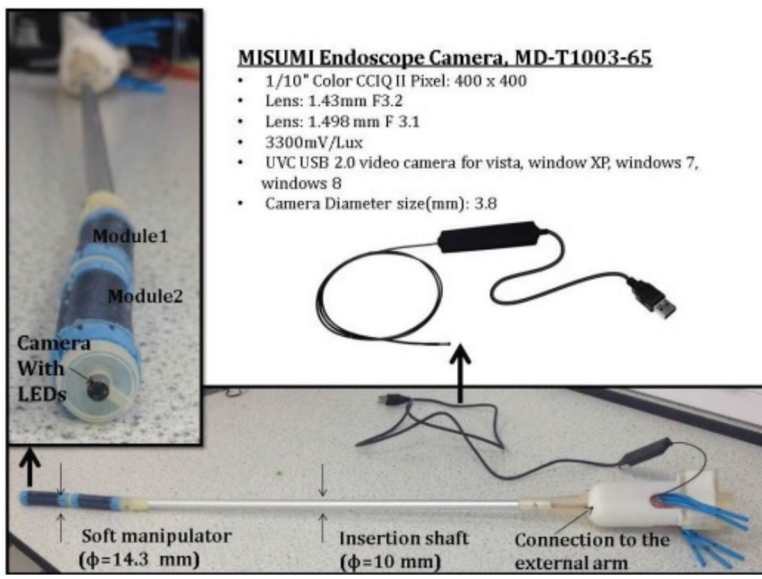

Figure 18.8 Soft two-module camera manipulator assembly and endoscopic camera details.

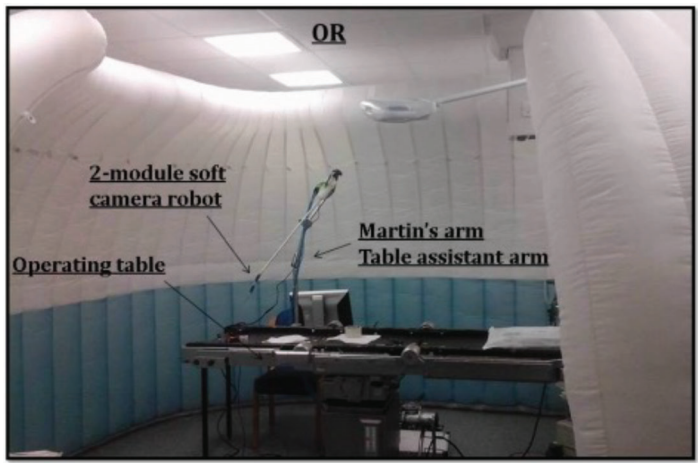

Figure 18.9 Panoramic view of the operating room (OR).

Figures 18.10 and 18.11 show pictures taken during the operations via laparoscopy on the human cadaver, performed at the Institute for Medical Science and Technology (IMSaT), University of Dundee, on October 13th, 2015 (carried out to appropriate ethical standards [2]).

The soft manipulator as well as other operative instruments and a supporting laparoscope have been inserted in the cadaver's inflated abdomen through a 15-mm trocar port. While one surgeon maneuvered the surgical

Figure 18.10 Surgeons controlling the soft camera manipulator and other laparoscopic devices.

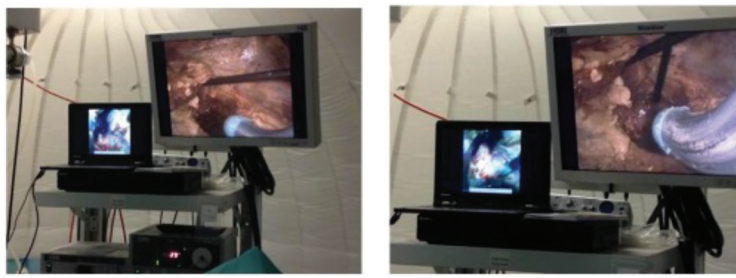

Figure 18.11 (Left) Vision of the target region through the soft camera module. (Right) Vision of the target region and soft manipulator through the laparoscope.

instruments, the other was using the joystick to control the STIFF-FLOP arm using the images from the robot's camera as feedback. Another surgeon guided a standard laparoscope to document the effective behavior of the soft manipulator underneath the abdominal wall (Figure 18.10). In Figure 18.11, the images from the endoscope (on the right screen) are shown and the images from the camera on the STIFF-FLOP manipulator (on the left screen) are also illustrated.

The STIFF-FLOP manipulator with camera confirmed its effectiveness in bringing a familiar endoscopic tool (as for example the camera) toward body areas which would not be accessible by standard straight and rigid laparoscopes. The soft and flexible nature of the manipulator demonstrated to be the key elements for reaching remote areas and overcome anatomical obstacles without damaging tissues and organs. Furthermore, thanks to the stable control of the pressure in the manipulator's pneumatic chambers, the surgeons were able to accomplish the relevant steps of the planned surgical procedure (the total mesorectal excision, TME).

Once the operation was complete, the camera was removed from the STIFF-FLOP arm prototype and the soft silicone elements were discarded.

References

[1] Abidi, H., Gerboni, G., Brancadoro, M., Fras, J., Diodato, A., and Cianchetti, M. et al. (2017). "Highly Dexterous 2-module Soft Robot for Intra-organ Navigation in Minimally Invasive Surgery", *Int. J. Med. Robot. Comput. Assist. Surg.* e1875.

[2] Arezzo, A., Mintz, Y., Allaix, M. E., et al. (2017). *Surg. Endosc.* 31:264.